Int J Appl Earth Obs Geoinformation 91 (2020) 102158

Contents lists available at ScienceDirect

Int J Appl Earth Obs Geoinformation

journal homepage: www.elsevier.com/locate/jag

Modeling and mapping aboveground biomass of the restored mangroves using ALOS-2 PALSAR-2 in East Kalimantan, Indonesia

Mst Karimon Nesha[a,*], Yousif Ali Hussin[a], Louise Marianne van Leeuwen[a], Yohanes Budi Sulistioadi[b]

[a] University of Twente, Faculty of Geo-Information Science and Earth Observation (ITC), Enschede, The Netherlands
[b] Mulawarman University, Climate, Soil and Water Conservation Laboratory, Forestry Faculty, Center of Geospatial Information Infrastructure Development (CGIID/PPIIG), Jl. Penajam Building B14 Kampus Gunung Kelua, Samarinda, Indonesia

ARTICLE INFO

Keywords:
Aboveground biomass (AGB)
Mangrove forests
HV polarization
Backscatter coefficients
ALOS-2 PALSAR-2
Linear regression model
K-fold CV
LLO CV

ABSTRACT

Accurate estimation of forest aboveground biomass (AGB) using remote sensing is a requisite for monitoring, reporting and verification (MRV) system of the United Nations Programme on Reducing Emissions from Deforestation and Forest Degradation. However, attaining high accuracy remains a great challenge in the diverse tropical forests. Among available technologies, L-band Synthetic Aperture Radar (SAR) estimates AGB with reasonably high accuracy in the terrestrial tropical forests. Nevertheless, the accuracy is relatively low in the mangrove forests. In this context, the study was carried out to model and map AGB using backscatter coefficients of Advanced Land Observing Satellite-2 (ALOS-2) Phased Array L-band SAR-2 (PALSAR-2) in part of the restored mangrove forest at Mahakam Delta, Indonesia. PALSAR-2 data was acquired with image scene observation during the peak low tide on 30 July 2018 from Japan Aerospace Exploration Agency. The forest parameters namely tree height and diameter at breast height were measured from 71 field plots in September-October 2018. The parameters were used in mangrove allometry to calculate the field AGB. Finally, HV polarized backscatter coefficients of PALSAR-2 were used to model AGB using linear regression. The model demonstrated a comparatively high performance using three distinct methods viz. independent validation (R^2 of 0.89 and RMSE of 23.16 tons ha^{-1}), random k-fold cross validation (R^2 of 0.89 and RMSE of 24.59 tons ha^{-1}) and leave location out cross validation (LLO CV) (R^2 of 0.88 and RMSE of 24.05 tons ha^{-1}). The high accuracy of the LLO CV indicates no spatial overfitting in the model. Thus, the model based on LLO CV was used to map AGB in the study area. This is the first study that successfully obtains high accuracy in modeling AGB in the mangrove forest. Therefore, it offers a significant contribution to the MRV mechanism for monitoring mangrove forests in the tropics and sub-tropics.

1. Introduction

Forests have a critical role in global climate regulation (Pan et al., 2011). Tropical forests are crucial in this regard as they sequester and store relatively large amounts of carbon compared to other forests. Moreover, mangroves sequester much more carbon per unit area than the terrestrial forests in the tropics (Donato et al., 2011). On the other hand, deforestation and forest degradation in the tropics contribute to 20 % of global anthropogenic CO_2 emissions each year (Gibbs and Herold, 2007; FFPRI, 2012). Again, mangroves alone account for 10 % emissions despite occupying only 0.7 % of the tropical forests (Giri et al., 2011).

As part of international efforts to reduce forest emissions, United Nations Programme on Reducing Emissions from Deforestation and Forest Degradation (UN-REDD) proposes an accurate measuring, reporting, and verification (MRV) mechanism of forest aboveground biomass (AGB) (Gibbs et al., 2007). Notably, the application of remote sensing (RS) techniques is central to realize the MRV mechanism of forest AGB (FFPRI, 2012).

When it comes to mangroves, studies mostly used optical RS for AGB estimation (Lu et al., 2004; Gibbs et al., 2007; Powell et al., 2010; Hirata et al., 2014; Dube and Mutanga, 2015). Nevertheless, optical RS

* Corresponding author. Present address: Laboratory of Geo-Information Science and Remote Sensing, Wageningen University and Research (WUR), Wageningen, The Netherlands.
E-mail addresses: karimonnesha@gmail.com, karimon.nesha@wur.nl (M.K. Nesha), y.a.hussin@utwente.nl (Y.A. Hussin), l.m.vanleeuwen@utwente.nl (L.M. van Leeuwen), bsulistioadi@fahutan.unmul.ac.id (Y.B. Sulistioadi).

https://doi.org/10.1016/j.jag.2020.102158
Received 2 September 2019; Received in revised form 2 May 2020; Accepted 11 May 2020
Available online 25 May 2020
1569-8432/ © 2020 The Authors. Published by Elsevier B.V. This is an open access article under the CC BY-NC-ND license (http://creativecommons.org/licenses/BY-NC-ND/4.0/).

has a major setback to directly quantify vegetation characteristics owing to its two-dimensional nature (Lucas et al., 2010). Besides, high accuracy is constrained by AGB saturation at a low level of the optical spectral bands (Lucas et al., 2015). Furthermore, the persistent clouds all year round makes it difficult to obtain clear optical images in the tropics (Asner, 2001).

LiDAR is an active RS technique correlated to AGB estimation with high accuracy (Duncanson et al., 2010). A vegetation specific spaceborne LiDAR, Global Ecosystem Dynamics Investigation (GEDI) is launched in December 2018 to capture forests in 3-dimension (3D) (Blumenfeld, 2020). Level 1 and Level 2 GEDI data are recently made available from January 2020 and Level 3 data will be available in mid-2020. Level 4 GEDI data associated with AGB values are expected to be available in early-2021 (Blumenfeld, 2020). However, clouds affect LiDAR data acquisition, and areas persistently covered by clouds may not be observed (Qi and Dubayah, 2016).

Radar, in contrast, is an active RS technique that can penetrate clouds, provide day and night imaging in all weather conditions (Asner, 2001). Moreover, Synthetic Aperture Radar (SAR) provides 3D vegetation data (Lucas et al., 2010), making it a potential tool for AGB estimation in the tropics on a large scale (Hyde et al., 2007; Kaasalainen et al., 2015). The long-wavelength L-band and P-band SAR are key for AGB estimation as they are related to volume scattering (Mermoz et al., 2014; Villard et al., 2016). Spaceborne P-band BIOMASS mission is yet to fly in 2022 (ESA, 2019). Therefore, L-band SAR has been widely used in tropical forests to date.

Nevertheless, only a handful of studies have been conducted for mangrove AGB estimation using L-band SAR (Hamdan et al., 2014; Pham and Yoshino, 2017; Pham et al., 2017, 2018). Besides, mangrove studies show comparatively much low accuracy as opposed to inland tropical forests (Mitchard et al., 2009; Nga, 2010; Odipo et al., 2016; Sumareke, 2016; Masolele, 2018). Moreover, mangrove AGB saturation is observed at a relatively low level ranging from 100 to 150 tons ha^{-1} (Lucas et al., 2007; Hamdan et al., 2014; Pham et al., 2018).

Notably, mangrove is a unique and complex forest with prop root systems, inundated during high tide and the ground is muddy during low tide (FAO, 2007). These unique attributes probably lead to high uncertainties in mangrove AGB estimation. Taking these uncertainties into account, we examined if cross (HV) and/or like (HH) polarized backscatter coefficients of Advanced Land Observing Satellite-2 (ALOS-2) Phased Array L-band SAR-2 (PALSAR-2) can model and map AGB with reasonable accuracy in the mangrove forest at Mahakam Delta, East Kalimantan, Indonesia. Additionally, we assessed the AGB saturation level in relation to backscatter coefficients of ALOS-2 PALSAR-2.

2. Data and methods

2.1. Study area

The study site covered approximately 105 ha between W longitude 117.560366° to E longitude 117.573216° and N latitude -0.533392° to S latitude -0.543048° at Mahakam Delta, East Kalimantan, Indonesia (Fig. 1). The dense mangrove vegetation of Mahakam Delta was converted into shrimp ponds starting in 1992 and until 2001, about 80 % of the mangroves were lost (Dutrieux, 2001). Nonetheless, plantation took place since 2002 to restore the mangroves (Sidik, 2008). The study site is in the restored mangroves in the sea-front areas at north distributary zones representing quite a homogenous vegetation structure. Noticeably, the site is intersected by Mahakam River, several water channels, and few shrimp ponds. *Avicennia alba* and *Rhizophora* spp. were the dominant tree species in the site (Appendix Fig. A1).

2.2. Data collection

2.2.1. Biometric data collection

The field data were collected from 71 circular plots of 500 m^2 (12.62 m radius) from 30 September to 24 October in 2018. The field plots were established using purposive sampling due to the constraints of accessibility and administrative permissions. Tree height and diameter at breast height (DBH) were measured from each plot for the trees with diameter > =10 cm. This is because trees < 10 cm in diameter have no significant contribution to AGB estimates (Brown, 2002).

According to Clough et al. (1997) and Chave et al. (2005), DBH should be measured above the prop roots of the *Rhizophora* spp. The main stem height over the prop roots varied. Measuring DBH at 1.3 m height from the buttress/stem base represented the main stem above the uppermost prop roots (Appendix Fig. A1). The height of *Rhizophora* spp. was measured from the prop roots on the ground to the top of the trees as prop roots contribute to the backscattering of the L-band SAR.

In the case of *Avicennia alba* and other tree species, DBH was measured at 1.3 m height from the ground (Appendix Fig. A1). There were many multi-stem trees of *Avicennia alba* and *Rhizophora* spp. In this case, each stem was considered as an individual tree (Clough et al., 1997). The wood density of the trees was collected from the archive of the World Agroforestry Indonesia database (World Agroforestry Indonesia, 2018). The wood density data of this archive was measured by Chave et al. (2005).

2.2.2. Acquisition of ALOS-2 PALSAR-2

One dual-polarized (HV and HH) PALSAR-2 image was obtained from the Japan Aerospace Exploration Agency (JAXA) through the Remote Sensing Technology Center of Japan. The image was right looking, ascending and single look complex (SLC) level 1.1 product acquired in stripmap mode with 4.29 m pixel spacing and 40.562° incidence angle. The image scene observation time was at 16:26 (UTC) on 30 July 2018 equivalent to local 01:26 a.m. representing the peak hours of the first low tide started at 12:28 a.m. Scene observation was chosen during the peak low tide to avoid the effects of inundation on PALSAR-2 backscattering. The total precipitation intensity at the Mahakam Delta region was 136.9 mm in July 2018 over 12 rainy days and it was 2.5 mm on 30 July following last rain on 22 July 2018 (Indriani et al., 2019).

2.3. Pre-processing of ALOS-2 PALSAR-2

The PALSAR-2 image was converted to retrieve HH and HV polarized backscatter coefficients known as normalized radar cross section (NRCS) and expressed in decibels (dB). The conversion was performed using Equation 1 proposed by Shimada et al. (2009) since it applies to the SLC level 1.1 PALSAR-2 product recommended by JAXA (JAXA, 2019).

Eq. (1): Retrieval of backscatter coefficients of ALOS-2 PALSAR-2.

$$\sigma^0 1.1\,\boldsymbol{product} = 10.\,\boldsymbol{log}10(\boldsymbol{I}^2 + \boldsymbol{Q}^2) + \boldsymbol{CF} - \boldsymbol{A}$$

Where:

$\boldsymbol{\sigma^0}$ **1.1** ***product*** = NRCS of SLC level 1.1 product in (dB)

I = Real part of SLC level 1.1product

Q = Imaginary part of SLC level 1.1product

CF = Calibration Factor = -83.0 dB

A = Constant, 32.0

Since the SLC SAR image is geometrically distorted (Small et al., 2009), Range-Doppler Terrain Correction (30 m) was applied to the PALSAR-2 image for geometric correction. The image was re-projected to the coordinate system of the study area (WGS_1984_UTM_Zone_50S). The corrected image had a pixel spacing of 7 m (Fig. 2a). Moreover, a Lee speckle filter with a kernel size of 3 × 3-pixel was applied to smooth the speckle noise (Fig. 2b).

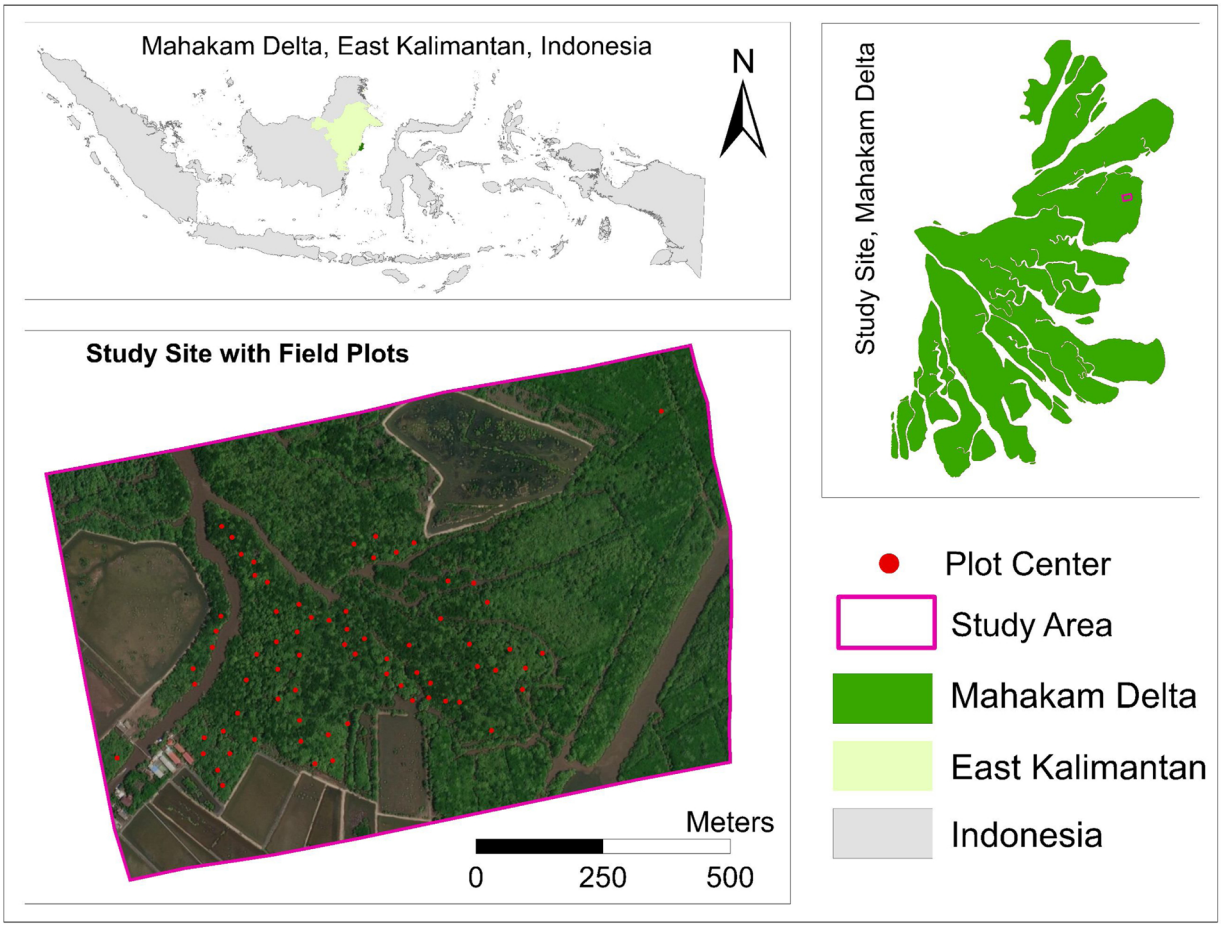

Fig. 1. Location of the study area with field plots indicated by red points (For interpretation of the references to colour in this figure legend, the reader is referred to the web version of this article).

2.4. Extraction of PALSAR-2 backscatter from field plots

The backscatter coefficients of PALSAR-2 were extracted from the field plots (25 m) using the 3 × 3-pixel window (21 m) as in Fig. 3 and Appendix Fig. A2. A similar approach was followed in previous studies (Hamdan et al., 2014; Sumareke, 2016; Masolele, 2018). The 4 × 4 or 5 × 5-pixel window reduces the error of excluding backscatter from the trees but smooths out the average backscatter within the plot (Sumareke, 2016). Moreover, many plots included nearby water body pixels in case of a 4 × 4 or 5 × 5-pixel window, further leveling out the average plot backscatter in our study site.

2.5. Field AGB calculation

The field AGB was calculated using tree height, DBH and wood density data in the allometry (Equation 2) proposed by Chave et al. (2005) for the mangrove forests. The allometry was most appropriate as we used wood density data developed by Chave et al. (2005). Utilizing tree height was another decisive factor to choose this allometry.

Eq. (2): Allometric equation for field AGB calculation.

$$\text{Mangroves, AGB} = 0.0509\,\rho\,\text{D}\hat{}2\,\text{H}$$

Where:

Mangroves, AGB = aboveground biomass of the mangroves

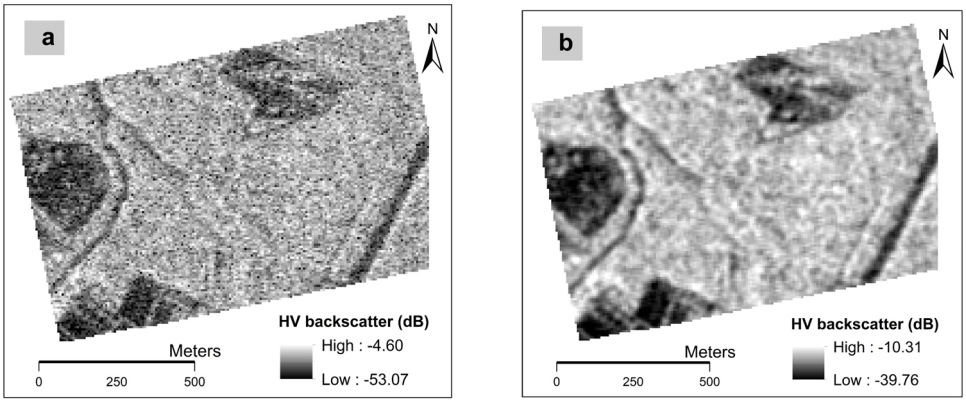

Fig. 2. HV polarized backscatter image after geometric correction (a) and speckle filtering (b).

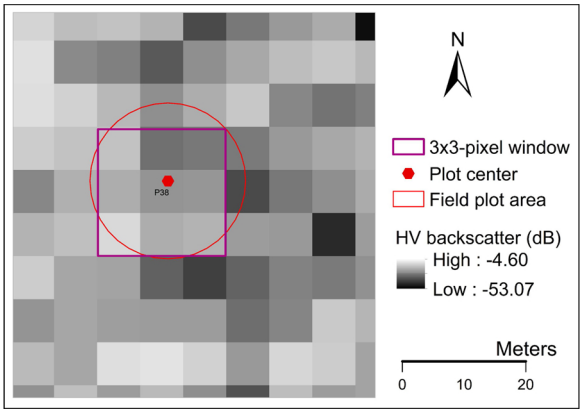

Fig. 3. A 3 × 3-pixel window on PALSAR-2 image for extraction of plot backscatter coefficients.

estimated in kilogram
D = tree DBH in centimeter
ρ = wood density in gcm^{-3}
H = tree height in meter

2.6. AGB and backscatter relationship

We applied a linear regression algorithm to estimate AGB using HH and/or HV backscatter coefficients and implemented in R environment for statistical programming (R Core Team, 2019). The linear algorithm was used as it demonstrated higher accuracy in estimating AGB. Likewise, our data met the requirements of linear regression (Moore et al., 2017). The accuracy of the relationship was assessed based on the coefficient of determination (R^2), root mean square error (RMSE) and p-value.

2.6.1. Model development, validation and accuracy assessment

The best performing relationship was used to model AGB. The model performance was evaluated using three different validation approaches. Initially, the dataset was randomly split into training and validation using 60:40 ratio. However, it can provide a bias model estimation as data in the validation set is lost for the training dataset. Moreover, accuracy fluctuates at every random model run.

Therefore, a repeated k-fold cross validation (CV) was applied where the entire dataset was randomly split into 5 equivalent folds. Then, five models were repetitively trained where one-fold data were held out during each model run. The held back data were used to assess the performance of the respective models. In this way, all data were used both for training and validation. Nevertheless, k-fold CV does not account for spatial overfitting.

Eventually, a target-oriented validation strategy, leave location out (LLO) CV was applied to address the spatial overfitting of the model. In this approach, the dataset was split again into five equal folds, but each test fold was formed using the data of a complete location (LLO). Thus, it predicted AGB outside the training locations. LLO CV was carried out in CAST package (Meyer et al., 2018b) and k-fold CV in caret package (Kuhn, 2019). An elaborate description and application of k-fold CV and LLO CV for the model prediction can be found in earlier studies (Micheletti et al., 2014; Gasch et al., 2015; Roberts et al., 2017; Meyer et al., 2016; Meyer et al., 2018a).

2.7. Determination of AGB saturation point

AGB saturation level was defined where a clear pattern of AGB leveling off was found on the logarithmic regression slope of the backscatter coefficients against the field AGB (Equation 3). This approach has been used in previous studies (Watanabe et al., 2006; Suzuki et al., 2013; Masolele, 2018). The highest performing relationship was used to determine the saturation level.

Eq. (3): Determination of AGB saturation point.

$$\text{Slope} = \Delta Y/\Delta X$$

Where:

ΔY is the change in the backscatter coefficients in relation to minimum backscatter coefficients and ΔX is the change in AGB with respect to minimum AGB value

2.8. AGB mapping

The model equation based on LLO CV was applied to PALSAR-2 where every pixel value was converted to AGB following the equation. A similar approach was followed for AGB mapping in the mangroves (Hamdan et al., 2014) and terrestrial tropical forests (Sumareke, 2016; Masolele, 2018).

3. Results and discussion

3.1. Descriptive results

The individual trees measured in the field plots totaled at 2407. Among them, *Avicennia alba* was the most dominating tree species accounting for approximately 60 %, followed by *Rhizophora* spp. at about 38 %. Few *Xylocarpus granatum* and *Bruguiera gymnorhiza* were also found. The field AGB ranged from 28.30 to 346.20 tons ha^{-1} with a mean of 136.30 tons ha^{-1}. The HV backscatter coefficients ranged from −23.01 to −14.54 dB.

3.2. AGB and backscatter relationship

The relationship between speckle filtered HV backscatter coefficients and AGB had a low accuracy at R^2 of 0.57 and RMSE of 46.01 tons ha^{-1} with p-value < 2.3e-14 (Fig. 4a). However, the non-

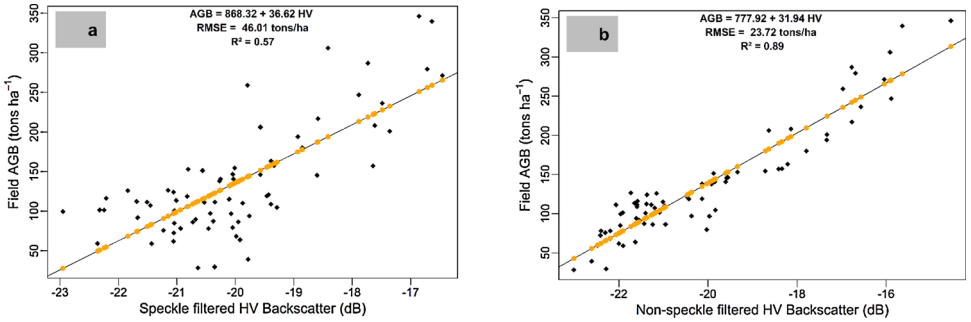

Fig. 4. Relationship of AGB with speckle filtered HV backscatter coefficients (a) and non-speckle filtered HV backscatter coefficients (b); black dots represent field AGB and orange dots depict predicted AGB.

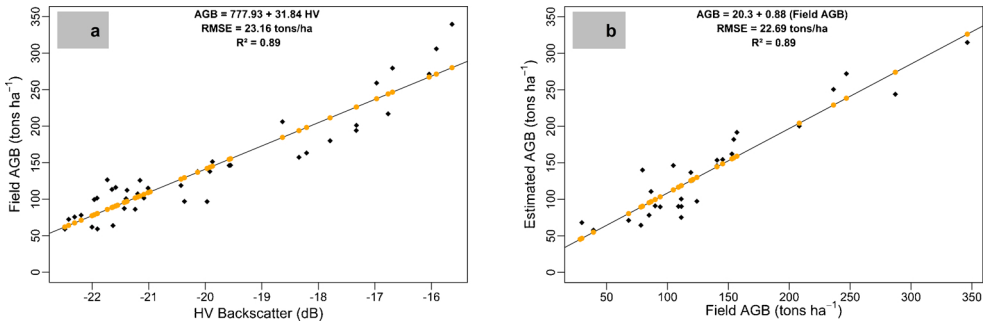

Fig. 5. AGB model using HV backscatter coefficients (a) and AGB model validation using field AGB and estimated AGB (b); black dots denote field AGB while orange dots represent predicted AGB.

speckle filtered HV backscatter coefficients demonstrated a high accuracy to estimate AGB at R^2 of 0.89 and RMSE of 23.72 tons ha^{-1} at p-value < 2.2e-16 (Fig. 4b). Therefore, we used non-speckle filtered backscatter coefficients for AGB estimation and referred to "backscatter coefficients" henceforth in this paper, if not stated otherwise.

The accuracy of AGB prediction using both HV and HH backscatter coefficients was also high at R^2 (adjusted) of 0.88 and RMSE of 23.63 tons ha^{-1} (p-value < 2.2e-16). On the contrary, the relationship between HH backscatter coefficients and field AGB was very weak at R^2 of 0.12 and RMSE of 66.07 tons ha^{-1} (p-value = 0.003).

3.2.1. Model development, validation and accuracy assessment

AGB was modeled using HV backscatter coefficients as it predicted AGB with higher accuracy. The model using 60 % dataset demonstrated a high accuracy at R^2 of 0.89 and RMSE of 23.16 tons ha^{-1} at p-value < 2.2e-16 (Fig. 5a). The model validation using an independent dataset (40 %) also depicted a comparable accuracy at R^2 of 0.89 and RMSE of 22. 69 tons ha^{-1} at p-value < 2.3e-14 (Fig. 5b). This means that the predictive performance of the model stayed intact when it was applied to an independent dataset.

Similarly, the model performance using random k-fold CV was parallel to the model performance using independent validation (Table 1). Again, the LLO CV model in relation to unknown locations depicted a comparable high accuracy (Table 1). The results of the LLO CV imply that the model was almost equally able to predict AGB outside the locations of the training data, thus overruling spatial overfitting.

To date, this is the first study to obtain such high accuracy in AGB estimation in the tropical mangrove forest using PALSAR-2. Among others, AGB estimation using non-speckle filtered HV backscatter coefficients largely contributed to high accuracy (Section 3.2, Fig. 4b). During speckle filtering, the values of water pixels and forest pixels were averaged which degraded the true backscatter coefficients from the mangroves (Fig. 2b) and eventually, resulted in low accuracy (Fig. 4a). Therefore, the use of speckle filter needs consideration where the forest is intersected by various water channels and it should not be applied at the expense of the actual forest backscatter coefficients.

Moreover, the enhanced backscattering from the mangrove forest has an important contribution to high accuracy in our study. This is linked to the scene observation time during peak hours of low tide when the forest is not inundated, but wet with high moisture content. The moisture content significantly increases the dielectric constant of objects (Richards, 2009). This, in turn, enhances the radar backscatter from the wet forests as observed in prior studies (Ormsby et al., 1985; Imhoff et al., 1986; Richards et al., 1987; Hussin, 1990; Wang et al., 1995; and Ling and Dai, 2012).

The mangrove forest in our study is approximately 16 years old similar to the studies in Vietnam (Pham and Yoshino, 2017; Pham et al., 2017, 2018) and Malaysia (Hamdan et al., 2014). However, the measurements of our forest parameters are comparatively high. This brings to the point of an increase in volume scattering with the growth of the trees (Le Toan et al., 1992). The tree growth strengthens the cross-polarization backscatter of L-band SAR as it can pass through the canopy down to the ground (Proisy, 2000).

Remarkably, our study area represents a naturally growing native plantation mangrove forest. Whereas, the mangrove is a managed planted forest in Malaysia (Hamdan et al., 2014) and Vietnam (Pham and Yoshino, 2017; Pham et al., 2017, 2018). These differences can lead to variation in forest growth and probably contribute to the relationship between backscatter coefficients and AGB.

Furthermore, 71 sample plots cover approximately all variations in our small and quite homogenous study area. This could conceivably contribute to the relatively high accuracy. While, AGB was estimated for the entire Matang mangrove forest (41,000 ha) using 320 sample plots (Hamdan et al., 2014). Again, 25 sample plots were used to estimate AGB of about 125 km mangrove forest in Vietnam (Pham and Yoshino, 2017; Pham et al., 2017, 2018)

In addition, high accuracy could be attributed to uncertainty reduction to a certain extent. For instance, we minimized scale mismatch by taking larger field plots than pixel window for backscatter extraction. Besides, there is no temporal difference between PALSAR-2 image and field data acquisition. Moreover, four additional measurements apart from the plot center were taken to ensure the geolocation of the plots. Details on uncertainty reduction can be found in previous studies (Réjou-Méchain et al., 2014, 2019).

3.3. Determination of AGB saturation point

AGB leveled off at 0.01 dB reaching 216.9 tons ha^{-1} on the logarithmic regression slope against the HV backscatter coefficients (Fig. 6). This implies that AGB was saturated at approximately 217 tons ha^{-1}. The AGB saturation level is comparatively much high in our study than that of earlier studies (Lucas et al., 2007; Hamdan et al., 2014; Pham et al., 2018). Since the PALSAR-2 scene was observed during the peak low tide, inundation does not induce saturation at a low AGB level in

Table 1
Model performance using independent validation (40 % dataset), k-fold CV and LLO CV.

Model	Validation	Intercept	Coefficient: HV backscatter	R^2	RMSE	P-value
AGB Model	Independent validation	777.93	31.84	0.89	23.16	< 2.2e-16
	K-fold CV	777.99	31.95	0.89	24.59	< 2.2e-16
	LLO CV	777.99	31.95	0.88	24.05	< 2.2e-16

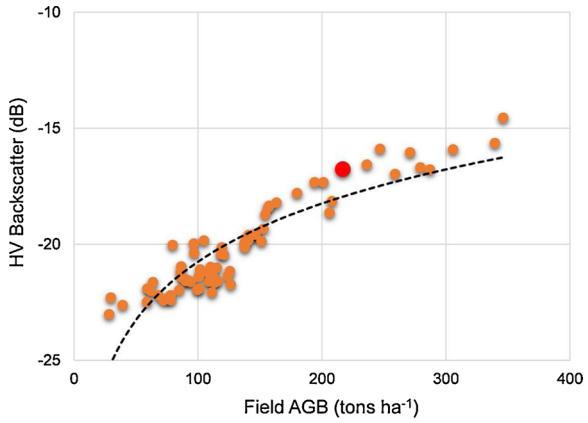

Fig. 6. AGB saturation level at 216.9 tons ha^{-1} indicated by the enlarged red-point.

our study as observed by Lucas et al. (2007).

3.4. AGB mapping

AGB was mapped in the study site (Fig. 7) using Equation, AGB = 777.99 + 31.95 HV derived from the LLO CV model (Table 1). The AGB estimates ranged between 1–350 tons ha^{-1} and totaled at 13,719 tons (Table 2 and Fig. 8). Most of the AGB varied from 100 to 200 tons ha^{-1} (25 ha), followed by 200 – 300 tons ha^{-1} (21 ha). Markedly, the estimated AGB range closely resembles the field AGB. The accuracy of the estimation was observed at R^2 of 0.89 and RMSE of 22.69 tons ha^{-1} (Fig. 5b). The range of AGB estimation is comparable to the findings by Hamdan et al. (2014), whilst the average is higher in our study. However, AGB estimation is higher in our study compared to the study by Pham et al. (2018).

4. Conclusions

Our study reveals that HV backscatter coefficients of PALSAR-2 model AGB in the restored mangrove forest at high accuracy with R^2 of 0.89 and RMSE of 23.16 tons ha^{-1}. Moreover, AGB saturation is found at a relatively higher level at around 217 tons ha^{-1}. The AGB estimation ranges between 1 – 350 tons ha^{-1} and strongly signifies the field

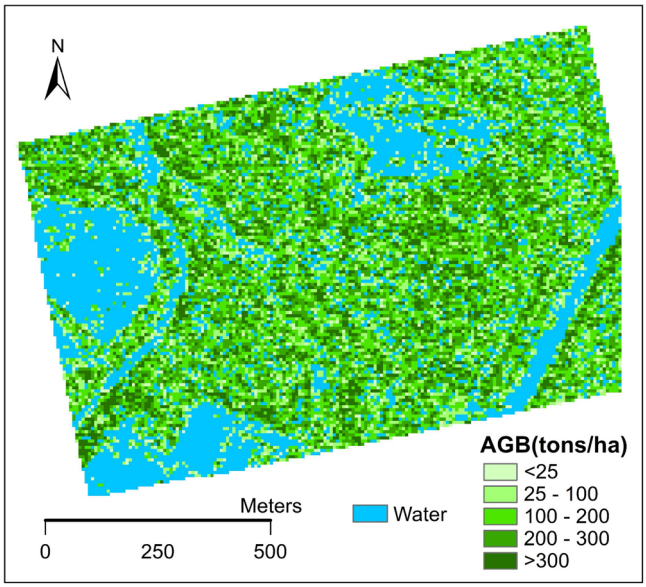

Fig. 7. AGB map of the study area. Water covers 30 ha crisscrossed the study site.

Table 2
Estimated AGB range with their corresponding area coverage in the study site.

AGB Range (tons ha^{-1})	Area (ha)	Total AGB (tons)
1 – 25	3.76	48.80
25 – 100	14.90	968.27
100 – 200	24.90	3773.57
200 – 300	21.07	5193.97
> 300	11.13	3734.09
Total	75.75	13,719

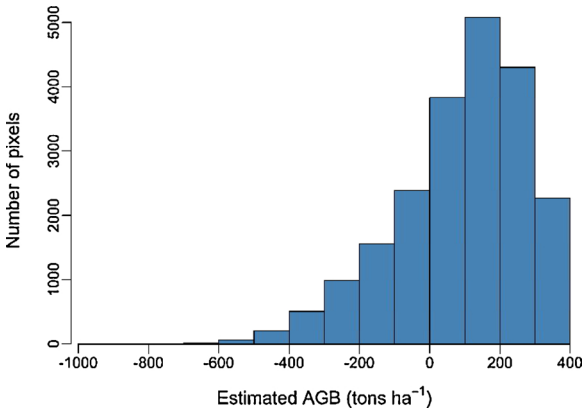

Fig. 8. Distribution of AGB estimated in the study area. The values > 0 represent AGB and the rest is water.

AGB in the study area. These findings suggest that cross-polarized backscatter coefficients have a great potential to estimate AGB with high accuracy in the restored and homogenous mangrove forests. Thus, our findings can contribute to the MRV system of the UN-REDD Programme.

Our model can be applied to other mangrove forests with similar biophysical characteristics. However, our model may not be applicable in the natural/non-restored mangroves with high AGB variation as the relationship may not be linear. Therefore, more research should be performed on natural mangroves where AGB varies significantly. With the availability of new RS data specifically GEDI LiDAR biomass and P-band SAR over the coming years, future studies might pave the way to address this gap. Future research should also focus on modeling AGB using multiple images to test the temporal consistency. Moreover, uncertainty assessment should be a crucial part of future investigations.

Declaration of competing interest

None.

Author's contributions

Mst Karimon Nesha developed the research concept, designed research methods, conducted fieldwork, processed and analyzed data, interpreted results, produced thesis report, drafted and revised the manuscript. **Yousif Ali Hussin,** the first supervisor, supervised at all stages of research work, thesis and manuscript writing. **L.M. van Leeuwen-de Leeuw,** the second supervisor, supervised research work and thesis writing. **Y. Budi Sulistioadi,** the third supervisor, supervised research work, especially fieldwork.

Acknowledgments

We humbly acknowledge that this work was financed by the Faculty of Geo-Information Science and Earth Observation (ITC), University of Twente, the Netherlands as part of the degree of Master of Science in Geo-information Science and Earth Observation for Mst Karimon

Nesha. We highly appreciate the Indonesian Ministry of Science and Technology and Higher Education to grant a research permit in Indonesia. We cordially thank Faculty of Forestry, Mulawarman University, Samarinda, Indonesia for their assistance in obtaining research permit and facilitating fieldwork and a special thanks to Muhammad Luthfi Hamdani and Mita Priskawanti for taking part in fieldwork. We express our gratitude to Prof. Dr. A.D. Nelson, Dr. Ling Chang and Prof. Dr. Larry Stillman for their valuable input. We are also very grateful to two anonymous reviewers for providing constructive comments to improve the manuscript.

Appendix A

.

A plot dominated by *Avicennia alba.*

A plot dominated by *Rhizophora spp.*

A plot adjoining a water canal.

A plot location indicated by the arrow next to Mahakam River.

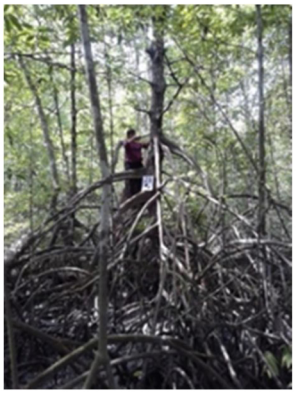

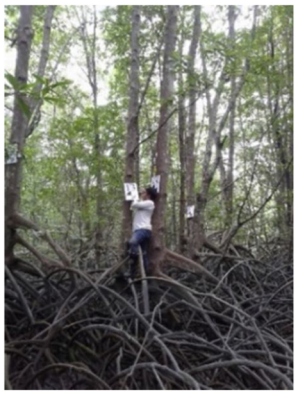

DBH measurement of *Rhizophora spp.* at 1.3m height from the stem junction.

DBH measurement of A*vicennia alba* at 1.3m height from the ground.

Fig. A1. Example photos of the field plots and data collection.

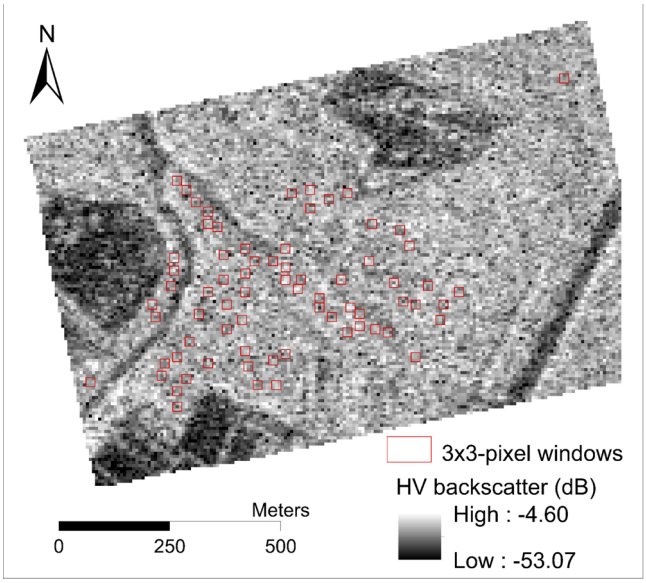

Fig. A2. The field plots indicated by 3 × 3-pixel windows on PALSAR-2 image.

Appendix B. Supplementary data

Supplementary material related to this article can be found, in the online version, at doi:https://doi.org/10.1016/j.jag.2020.102158.

References

Asner, G.P., 2001. Cloud cover in landsat observations of the brazilian amazon. Int. J. Remote Sens. 22 (18), 3855–3862.

Blumenfeld, J., 2020. Earth in the Third Dimension: First GEDI Data. Available. Retrieved March 6, 2020, from. https://earthdata.nasa.gov/learn/articles/first-gedi-data-available.

Brown, S., 2002. Measuring carbon in forests: current status and future challenges. Environ. Pollut. 116 (3), 363–372.

Chave, J., Andalo, C., Brown, S., Cairns, M.A., Chambers, J.Q., Eamus, D., Yamakura, T., 2005. Tree allometry and improved estimation of carbon stocks and balance in tropical forests. Oecologia 145 (1), 87–99.

Clough, B.F., Dixon, P., Dalhaus, O., 1997. Allometric relationships for estimating biomass in multi-stemmed mangrove trees. Aust. J. Bot. 45 (6), 1023.

Donato, D.C., Kauffman, J.B., Murdiyarso, D., Kurnianto, S., Stidham, M., Kanninen, M., 2011. Mangroves among the most carbon-rich forests in the tropics. Nat. Geosci. 4 (5), 293–297.

Dube, T., Mutanga, O., 2015. Evaluating the utility of the medium-spatial resolution Landsat 8 multispectral sensor in quantifying aboveground biomass in uMgeni catchment, South Africa. Isprs J. Photogramm. Remote. Sens. 101, 36–46.

Duncanson, L.I., Niemann, K.O., Wulder, M.A., 2010. Estimating forest canopy height and terrain relief from GLAS waveform metrics. Remote Sens. Environ. 114 (1), 138–154.

Dutrieux, E., 2001. The mahakam delta environment. From the 80s up to now: a synthesis of 15-year investigation. In: Kusumastanto, T., Bengen, D.G., Widigdo, B., Soeseno, I. (Eds.), Optimizing Development and Environmental Issues at Coastal Area: Problem and Solution for Sus.

ESA, 2019. ESA-Biomass. Retrieved March 6, 2020, from. https://www.esa.int/Applications/Observing_the_Earth/The_Living_Planet_Programme/Earth_Explorers/Biomass.

FAO, 2007. The World's Mangroves 1980-2005. Retrieved August 15, 2018, from. https://forestsnews.cifor.org/31178/indonesian-mangroves-special-fact-file-a-global-treasure-under-threat?fnl=en.

FFPRI, 2012. REDD Plus Cookbook: How to Measure and Monitor Forest Carbon. Tsukuba, Japan. .

Gasch, C.K., Hengl, T., Gräler, B., Meyer, H., Magney, T.S., Brown, D.J., 2015. Spatio-temporal interpolation of soil water, temperature, and electrical conductivity in 3D + T: the Cook Agronomy Farm data set. Spat. Stat. 14, 70–90.

Gibbs, H.K., Herold, M., 2007. Tropical deforestation and greenhouse gas emissions. Environ. Res. Lett. 2 (4), 045021.

Gibbs, H.K., Brown, S., Niles, J.O., Foley, J.A., 2007. Monitoring and estimating tropical forest carbon stocks: making REDD a reality. Environ. Res. Lett. 2 (2007), 045023.

Giri, C., Ochieng, E., Tieszen, L.L., Zhu, Z., Singh, A., Loveland, T., Duke, N., 2011. Status and distribution of mangrove forests of the world using earth observation satellite data. Glob. Ecol. Biogeogr. 20 (1), 154–159.

Hamdan, O., Aziz, H.K., Hasmadi, I.M., 2014. L-band ALOS PALSAR for biomass estimation of matang mangroves, Malaysia. Remote Sens. Environ (April 2018).

Hirata, Y., Tabuchi, R., Patanaponpaiboon, P., Poungparn, S., Yoneda, R., Fujioka, Y., 2014. Estimation of aboveground biomass in mangrove forests using high-resolution satellite data. J. For. Res. 19 (1), 34–41.

Hussin, Y.A., 1990. The Effects of Polarization and Incidence Angle on Radar Backscatter From Forest Cover. Colorado State University, Fort Collins.

Hyde, P., Nelson, R., Kimes, D., Levine, E., 2007. Exploring LiDAR–RaDAR synergy—-predicting aboveground biomass in a southwestern ponderosa pine forest using LiDAR, SAR and InSAR. Remote Sens. Environ. 106 (1), 28–38.

Imhoff, M., Story, M., Vermillion, C., Khan, F., Polcyn, F., 1986. Forest canopy characterization and vegetation penetration assessment with space-borne radar. Ieee Trans. Geosci. Remote. Sens. (4), 535–542 GE-24.

Indriani, N., Devina, A.C., Sari, P., 2019. Kota Samarinda Dalam Angka 2019. Samarinda. Retrieved from. https://samarindakota.bps.go.id/.

JAXA, 2019. Calibration Result of ALOS-2/PALSAR-2 JAXA Standard Products. Retrieved March 5, 2020, from. https://www.eorc.jaxa.jp/ALOS-2/en/calval/calval_index.htm.

Kaasalainen, S., Holopainen, M., Karjalainen, M., Vastaranta, M., Kankare, V., Karila, K., Osmanoglu, B., 2015. Combining Lidar and synthetic aperture radar data to estimate forest biomass: status and prospects. Forests 6 (12), 252–270.

Kuhn, M., 2019. Caret: Classification and Regression Training. R Package Version 6. 0-82. .

Le Toan, T., Beaudoin, A., Riom, J., Guyon, D., 1992. Relating forest biomass to SAR data. Ieee Trans. Geosci. Remote. Sens. 30 (2), 403–411.

Ling, F., Dai, Y., 2012. Understanding the enhanced backscatter of coastal forest plantation in L-band synthetic aperture radar images. In: 2012 First International Conference on Agro- Geoinformatics (Agro-Geoinformatics). IEEE. pp. 1–4.

Lu, D., Mausel, P., Brondízio, E., Moran, E., 2004. Relationships between forest stand parameters and Landsat TM spectral responses in the Brazilian Amazon Basin. For. Ecol. Manage. 198 (1–3), 149–167.

Lucas, R.M., Mitchell, A.L., Rosenqvist, A., Proisy, C., Melius, A., Ticehurst, C., 2007. The potential of L-band SAR for quantifying mangrove characteristics and change: case studies from the tropics. Aquat. Conserv. Mar. Freshw. Ecosyst. 17 (3), 245–264.

Lucas, R.M., Lee, A., Armston, J., Carreiras, J., Viergever, K., Bunting, P., Woodhouse, I., 2010. Quantifying carbon in savannas. Ecosystem Function in Savannas. CRC Press, pp. 155–174. https://doi.org/10.1201/b10275-12.

Lucas, R.M., Mitchell, A.L., Armston, J., 2015. Measurement of forest above-ground biomass using active and passive remote sensing at large (Subnational to global) scales. Curr. For. Rep. 1 (3), 162–177.

Masolele, R. N. (2018). *ALOS-2 PALSAR-2 L-band cross-polarized radar data analysis for modelling above-ground biomass/ carbon stock and carbon sequestration of tropical rainforest, Berkelah, Malaysia (MSc Thesis)*. Faculty of Geo-Information and Earth Observation (ITC), University of Twente, The Netherlands. Retrieved from http://www.itc.nl/library/papers_2018/msc/nrm/masolele.pdf.

Mermoz, S., Rejou-Mechain, M., Villard, L., Le Toan, T., Rossi, V., Gourlet-Fleury, S., 2014. Biomass of dense forests related to L-band SAR backscatter? In: 2014 IEEE

Geoscience and Remote Sensing Symposium. IEEE. pp. 1037–1040.
Meyer, H., Katurji, M., Appelhans, T., Müller, M., Nauss, T., Roudier, P., Zawar-Reza, P., 2016. Mapping daily air temperature for Antarctica based on MODIS LST. Remote Sens. (Basel) 8 (9), 732.
Meyer, H., Reudenbach, C., Hengl, T., Katurji, M., Nauss, T., 2018a. Improving performance of spatio-temporal machine learning models using forward feature selection and target-oriented validation. Environ. Model. Softw. 101, 1–9.
Meyer, H., Reudenbach, C., Ludwig, M., Nauss, T., 2018b. CAST: "Caret" Applications for Spatial-temporal Models. R Package Version 0.3.1.
Micheletti, N., Foresti, L., Robert, S., Leuenberger, M., Pedrazzini, A., Jaboyedoff, M., Kanevski, M., 2014. Machine learning feature selection methods for landslide susceptibility mapping. Math. Geosci. 46 (1), 33–57.
Mitchard, E.T.A., Saatchi, S.S., Woodhouse, I.H., Nangendo, G., Ribeiro, N.S., Williams, M., Meir, P., 2009. Using satellite radar backscatter to predict above-ground woody biomass: a consistent relationship across four different African landscapes. Geophys. Res. Lett. 36 (23), L23401.
Moore, D.S., McCabe, G.P., Craig, B.A., 2017. Introduction to the Practice of Statistics, 9th ed. W.H. Freeman and Company, a Macmillan Higher Education Company, New York.
Nga, T.N., 2010. Estimation and Mapping of Above Ground Biomass for the Assessment and Mapping of Carbon Stocks in Tropical Forest Using SAR Data- a Case Study in Afram Estimation and Mapping of Above Ground Biomass for the Assessment and Mapping of Carbon Stocks in Tropi. Earth Observation (ITC), University of Twente, The Netherlands.
Odipo, V., Nickless, A., Berger, C., Baade, J., Urbazaev, M., Walther, C., Schmullius, C., 2016. Assessment of aboveground woody biomass dynamics using terrestrial laser scanner and L-Band ALOS PALSAR data in south african savanna. Forests 7 (12), 294.
Ormsby, J.P., Blanchard, B.J., Blanchard, A.J., 1985. Detection of lowland flooding using active microwave systems. Photogramm. Eng. Remote Sensing 51 (3).
Pan, Y., Birdsey, R.A., Fang, J., Houghton, R., Kauppi, P.E., Kurz, W.A., Hayes, D., 2011. A large and persistent carbon sink in the world's forests. Science 333 (6045), 988–993.
Pham, T.D., Yoshino, K., 2017. Aboveground biomass estimation of mangrove species using ALOS-2 PALSAR imagery in Hai Phong City, Vietnam. J. Appl. Remote Sens. 11 (2), 026010.
Pham, T.D., Yoshino, K., Bui, D.T., 2017. Biomass estimation of Sonneratia caseolaris (l.) Engler at a coastal area of Hai Phong city (Vietnam) using ALOS-2 PALSAR imagery and GIS-based multi-layer perceptron neural networks. GIsci. Remote Sens. 54 (3), 329–353.
Pham, T.D., Yoshino, K., Le, N.N., Bui, D.T., 2018. Estimating aboveground biomass of a mangrove plantation on the Northern coast of Vietnam using machine learning techniques with an integration of ALOS-2 PALSAR-2 and Sentinel-2A data. Int. J. Remote Sens. 39 (22), 7761–7788.
Powell, S.L., Cohen, W.B., Healey, S.P., Kennedy, R.E., Moisen, G.G., Pierce, K.B., Ohmann, J.L., 2010. Quantification of live aboveground forest biomass dynamics with Landsat time-series and field inventory data: a comparison of empirical modeling approaches. Remote Sens. Environ. 114 (5), 1053–1068.
Proisy, C., 2000. Interpretation of polarimetric radar signatures of mangrove forests. Remote Sens. Environ. 71 (1), 56–66.
Qi, W., Dubayah, R.O., 2016. Combining Tandem-X InSAR and simulated GEDI lidar observations for forest structure mapping. Remote Sens. Environ. 187, 253–266. https://doi.org/10.1016/j.rse.2016.10.018.
R Core Team, 2019. R: a Language and Environment for Statistical Computing. R Foundation for Statistical Computing, Vienna, Austria. http://www.r-project.org/index.html.
Réjou-Méchain, M., Muller-Landau, H.C., Detto, M., Thomas, S.C., Le Toan, T., Saatchi, S.S., Chave, J., 2014. Local spatial structure of forest biomass and its consequences for remote sensing of carbon stocks. Biogeosciences 11 (23), 6827–6840.
Réjou-Méchain, Maxime, Barbier, N., Couteron, P., Ploton, P., Vincent, G., Herold, M., Pélissier, R., 2019. Upscaling forest biomass from field to satellite measurements: sources of errors and ways to reduce them. Surv. Geophys. 40 (4), 881–911.
Richards, John A., 2009. Remote Sensing With Imaging Radar. Springer, Berlin Heidelberg.
Richards, J.A., Woodgate, P.W., Skidmore, A.K., 1987. An explanation of enhanced radar backscattering from flooded forests. Int. J. Remote Sens. 8 (7), 1093–1100.
Roberts, D.R., Bahn, V., Ciuti, S., Boyce, M.S., Elith, J., Guillera-Arroita, G., Dormann, C.F., 2017. Cross-validation strategies for data with temporal, spatial, hierarchical, or phylogenetic structure. Ecography 40 (8), 913–929.
Shimada, M., Isoguchi, O., Tadono, T., Isono, K., 2009. PALSAR radiometric and geometric calibration. Ieee Trans. Geosci. Remote. Sens. 47 (12), 3915–3932.
Sidik, A.S., 2008. The change of mangrove ecosystem in mahakam delta, Indonesia: a complex social-environment pattern of linkages in resources utilization. In: The South China Sea: Susutaining Ocean Productivities, Maritime Communities and the Climate Conference. Kuantan, Malaysia.
Small, D., Jehle, M., Schubert, A., Meier, E., 2009. Accurate Geometric Correction for Normalisation of PALSAR Radiometry.
Sumareke, A.M., 2016. Modelling and mapping aboveground biomass and carbon stock using alos-2 palsar-2 data. Ayer Hitam Tropical Rainforest Reserve in Malaysia. ITC, University of Twente, The Netherlands Msc thesis.
Suzuki, R., Kim, Y., Ishii, R., 2013. Sensitivity of the backscatter intensity of ALOS/PALSAR to the above-ground biomass and other biophysical parameters of boreal forest in Alaska. Polar Sci. 7 (2), 100–112.
Villard, L., Le Toan, T., Ho Tong Minh, D., Mermoz, S., Bouvet, A., 2016. Forest biomass from radar remote sensing. Land Surface Remote Sensing in Agriculture and Forest. pp. 363–425.
Wang, Yong, Hess, L.L., Filoso, S., Melack, J.M., 1995. Understanding the radar backscattering from flooded and nonflooded Amazonian forests: results from canopy backscatter modeling. Remote Sens. Environ. 54 (3), 324–332.
Watanabe, M., Shimada, M., Rosenqvist, A., Tadono, T., Matsuoka, M., Romshoo, S.A., Moriyama, T., 2006. Forest structure dependency of the relation between L-Bandsigma0and biophysical parameters. Ieee Trans. Geosci. Remote. Sens. 44 (11), 3154–3165.
World Agroforestry Indonesia, 2018. Database: Wood Density. Retrieved December 2, 2018, from. http://www.worldagroforestry.org/output?field_type_tid=63.